energies

MDPI

Article

Application Properties of ZnO and AZO Thin Films Obtained by the ALD Method

Barbara Swatowska [1,*], Wiesław Powroźnik [1], Halina Czternastek [2], Gabriela Lewińska [1], Tomasz Stapiński [1], Rafał Pietruszka [3], Bartłomiej S. Witkowski [3] and Marek Godlewski [3]

[1] Department of Electronics, Faculty of Computer Science, Electronics and Telecommunications, AGH University of Science and Technology, 30-059 Krakow, Poland; wpowroz@agh.edu.pl (W.P.); glewinska@agh.edu.pl (G.L.); stap@agh.edu.pl (T.S.)
[2] Institute of Physics, Pedagogical University of Cracow, ul. Podchorążych 2, 30-084 Krakow, Poland; czternas@agh.edu.pl
[3] Institute of Physics, Polish Academy of Sciences, Al. Lotników 32/46, 02-668 Warsaw, Poland; pietruszka@ifpan.edu.pl (R.P.); bwitkow@ifpan.edu.pl (B.S.W.); godlew@ifpan.edu.pl (M.G.)
* Correspondence: swatow@agh.edu.pl; Tel.: +48-126-173-039; Fax: +48-126-332-398

Abstract: The thin layers of ZnO and ZnO: Al (Al doped zinc oxide—AZO) were deposited by the atomic deposition layer (ALD) method on silicon and glass substrates. The structures were deposited using diethylzinc (DEZ) and deionized water as zinc and oxygen precursors. A precursor of trimethylaluminum (TMA) was used to introduce the aluminum dopant. The present study of ALD-deposited ZnO and AZO films was motivated by their applications in photovoltaics. We attempted to expose several properties of such films. Structural, optical (including ellipsometric measurements) and electrical investigations were performed. We discussed the relations between samples doped with different Al fractions and their properties.

Keywords: AZO thin films; ALD technique; optical properties; structural properties; electrical parameters

Citation: Swatowska, B.; Powroźnik, W.; Czternastek, H.; Lewińska, G.; Stapiński, T.; Pietruszka, R.; Witkowski, B.S.; Godlewski, M. Application Properties of ZnO and AZO Thin Films Obtained by the ALD Method. *Energies* **2021**, *14*, 6271. https://doi.org/10.3390/en14196271

Academic Editor: Cuma Tyszkiewicz

Received: 13 August 2021
Accepted: 27 September 2021
Published: 1 October 2021

1. Introduction

Zinc oxide (ZnO) is one of the most popular semiconductor materials with a wide band gap equal to 3.27 eV at room temperature, with an exciton binding energy of 60 meV, but most of all, with a free electron concentration regulated in a wide range, up to 10^{20} cm^{-3} [1–3]. Due to such properties, ZnO-based thin layers can be used as the transparent conducting oxide (TCO) in solar cells and in ultraviolet light emitters [1–3].

ZnO films when used for TCO applications [4] can replace the widely used indium tin oxide (ITO). Even though ITO layers are still superior—they have high conductivity and optical transparency in the wide range of the solar spectrum [4,5]—their price becomes too high due to the increasing price of indium. This fact started an active search for alternative TCO materials [4,6]. One of the most promising alternative TCO materials is ZnO, in particular when doped with Al (AZO), Ga (GZO), In (IZO) or F (FZO) [4].

In the present study we concentrate on AZO films deposited by the atomic layer deposition (ALD) technique. Such films can be deposited using a variety of techniques, including most of all magnetron sputtering [7], pulsed laser deposition [8], chemical vapor deposition [9] and sol–gel deposition [10,11].

To select the growth method of ZnO (AZO) films, several parameters must be taken into account, especially the required TCO parameters [12], but also price, the possibility of low temperature growth and scalability to large substrates as well. This is why PLD is not used in industrial processes despite the best electrical parameters of the PLD films. Magnetron sputtering is the most commonly used deposition technique. The so-obtained layers show resistivity on the order of 10^{-4} Ω cm, with optical transparency >80% in the visible spectrum [13]. The reported AZO film resistivity and transparency (above 80% in

the visible light range) are very close to those of ITO. Thus, AZO films are successfully used as transparent electrodes in silicon-based (see e.g., [14]) or copper indium gallium diselenide (CIGS) solar cells [15].

Recently, ALD technology has attracted a lot of attention. Increasing interest in ALD is related to the unique capability with the possibility of deposition of pinhole free conformal layers on flat or textured surface, low temperature deposition and scalability to large surfaces [16–18]. Properties of ZnO films grown by ALD at low temperature (LT) were discussed by us in detail in our previous works [19,20]. Due to the self-limited growth rate, the layer thickness can be controlled with a precision of ~1 nm by controlling the number of ALD cycles. The combination of these features allows for the production of new, unique and nano-scale optoelectronic devices [21]. However, despite the first industrial applications, basic research is still needed to understand the dependencies between growth parameters and structural, electrical and optical properties of the films. The latter is well documented by our investigations of ALD-grown ZnO films in which we observed a range of puzzling film properties both for ZnO [22–24], as well as AZO films [25,26]. We list here only a few puzzling properties of these films. For example, why does the growth mode of AZO films change with an increase of Al fraction in the films [25]? Is the growth epitaxial or it is depositional [23]? Why do we observe a large shift of an optical band gap with increasing Al fraction in the films [25]?

This work attempts to clear up some of these questions. ZnO layers and Al doped ZnO layers with different concentrations of Al are grown using ALD and doping procedures described in the literature [25,26]. These layers were tested by means of X-ray diffraction (XRD), scanning electron microscopy (SEM), energy-dispersive X-ray spectroscopy (EDS), optical spectrophotometry and spectroscopic ellipsometry (SE). Electrical measurements (Hall effect studies) were also performed to obtain data on electron concentration and their mobility.

2. Materials and Methods

2.1. Sample Preparation

ALD layers were deposited on silicon and glass substrates. A high-resistance 4" (100) Czochralski silicon wafer (Cz-Si) was cut into pieces of size 1 × 1 cm^2 for SEM measurement and 2.5 × 2.5 cm^2 for structural measurements (XRD and ellipsometry). The glass substrates (bought from Carl Rothe, Karlsruhe, Germany, id. 0656.1) were cut into pieces of size 2.5 × 2.5 cm^2 for optical study. Prior to deposition processes, the substrates were cleaned using our standard procedure, first in acetone, and then in isopropanol and deionized water for 5 min in an ultrasonic cleaner. After cleaning, the samples were blow-dried using 5N purity nitrogen.

ALD Layer Deposition

The layers were deposited on silicon and glass substrates using a Beneq TSF 200 commercial ALD reactor. A rotary vane pump allowed us to keep the pressure in the growth chamber at ~3 × 10^{-1} Torr. The temperature during the growth of all samples was kept at 160 °C. Our earlier investigations indicated that films deposited at this temperature are of a relatively good crystallographic quality and show relatively high free electron concentrations and low deep defect concentrations [23,24]. A higher temperature (200 °C) was used in a previous study [25,26]. The zinc oxide and aluminum doped zinc oxide layers were grown using diethylzinc (DEZ; CAS: 557-20-0) and trimethylaluminum (TMA; CAS: 75-24-1) as zinc and aluminum precursors, respectively. Deionized water was used as the precursor of oxygen [25,26]. During the growth process, diethylzinc, trimethylaluminum and deionized water were kept at room temperature (22 ± 2 °C). These precursors were sequentially introduced into the growth chamber using pure nitrogen (5N purity) as a carrier gas. Each ALD cycle included four steps: (i) pulse of the first reagent (precursor), (ii) purge of the growth chamber by an inert gas, (iii) pulse of the second reagent, (iv) purge of the growth chamber by an inert gas. We used 1 s or 2 s purging times. This may have affected the

growth mode of the layers since we found that for longer purging times (we tested for times up to 12 s) the growth on the c-axis perpendicular to the surface was preferential [23]. The technological details of layer growth are summarized in Table 1.

Table 1. The ALD growth parameters of ZnO and AZO layers.

Layer	Reagent	Pulse (s)	Purge (s)	Ratio of ALD Cycles
ZnO	DEZ	0.04	1	
	H_2O	0.02	1	
AZO	TMA	0.04	1	1:*m*
	H_2O	0.02	2	
	DEZ	0.04	1	$(1 \times TMA + H_2O + m \times DEZ + H_2O)$
	H_2O	0.02	1	

A zinc oxide layer was deposited introducing the DEZ and H_2O precursors alternately. For the growth of AZO layers, the following solution was used: To obtain the AZO layer, ***m*** (DEZ + $H_2O \rightarrow$ ZnO) cycles were separated by one (TMA + $H_2O \rightarrow Al_2O_3$) cycle. In this case, ***m*** equaled 7, 9, 19 and 29. This approach allowed us to obtain a ZnO layer with different Al dopant concentrations. If the number of ***m*** is small, the aluminum content in the ZnO is high. As the value of ***m*** increases, the concentration of dopant decreases. To initiate growth, we started first with a TMA pulse, as in our previous study [25,26]. Figure 1 shown below shows the method of doping in the ALD technology.

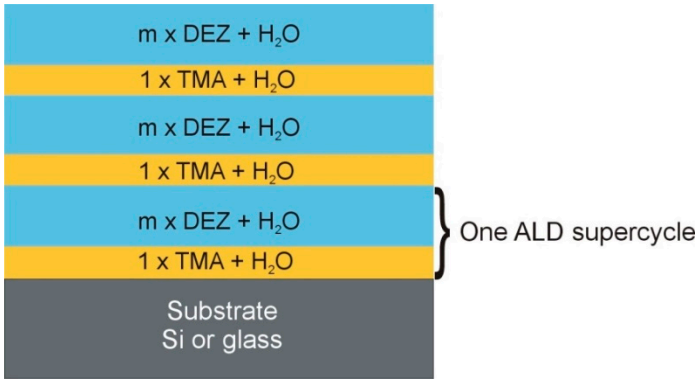

Figure 1. Doping procedure used in ALD technology to obtain AZO films.

ALD "supercycle" was repeated to obtain films with about 200 nm thickness.

2.2. Measurement Techniques

A NanoCalc 2000 thin film reflectometer (Ocean Optics, Inc., Rochester, NY, USA) was used to measure the thickness of the layers deposited on Si. Additionally, the thickness of each film was determined from SEM cross-section images. These values were then confirmed by ellipsometric measurements. The cross sections, top view images and EDS spectra were measured using a Hitachi SU-70 scanning electron microscope (SEM), at an accelerating voltage of 5 kV (EDS) and 15 kV (images). For these investigations, films deposited on silicon substrates were used.

An X'pert MPD (Panalytical) X-ray diffractometer (A.P. Instruments Sp.z o.o. Sp.k., Warszawa, Poland) with CuK_α = 1.5425 Å radiation was used to investigate the structural properties of thin films of ZnO and AZO deposited on Si substrates. The $\theta/2\theta$ scans of the films were collected in the 2θ angle range from 25 to 115 degrees.

The electrical parameters of zinc oxide (ZnO) and aluminum doped zinc oxide (AZO) were measured by RT Hall in the van der Pauw configuration. A permanent magnet from RH2035PhysTech system provided a magnetic field of 0.4 T. Hall measurements were

carried out on layers deposited onto glass substrates (1 × 1 cm^2) to avoid the influence of Si substrate on electrical parameters.

The variable angle spectroscopic ellipsometry measurements for four incident angles, namely 60°, 65°, 70° and 75°, were carried out using a spectroscopic ellipsometer (M-2000, J.A. Woollam Co. Inc., Lincoln, NE, USA) following the method described in [27–29]. The measurements of Ψ—amplitude component, and Δ—phase shift as a function of wavelength λ, in the range from 300 to 1700 nm provided refractive index n and extinction coefficient k dispersion relations. The ellipsometric modeling was performed using Complete EASE Data Acquisition and Analysis Software for Spectroscopic Ellipsometers (J.A. Woolam Co. Inc., Lincoln, NE, USA) [30].

Optical transmission and reflectance of ZnO and AZO layers were measured by means of a Perkin-Elmer Lambda 19 spectrophotometer (PerkinElmer Polska sp. z o.o., Krakow, Poland) (range from 250 to 1700 nm).

3. Results

The first important question to be answered was if the "doping" method" used by us (sequences of pulses of two metal precursors) really leads to Al doped films. Importantly, we did not used postgrowth annealing as in reference [26] to improve Al inter-diffusion. To answer this question, we performed EDS investigations of AZO films deposited on an Si substrate. Elemental composition of the analyzed structures, as determined from EDS investigations (different areas of samples were tested), are listed in Table 2.

Table 2. Values of m (DEZ + H_2O → ZnO) cycles and elemental composition of thin ZnO and AZO layers obtained by the ALD method on silicon substrates.

	ZnO	AZO-1	AZO-2	AZO-3	AZO-4
m	0	29	19	9	7
Al (%)	0	1.6	2.5	6.3	7.9
Zn (%)	54.2	51.4	50.5	45.1	42.8
O (%)	45.8	47.0	47.0	48.6	49.3
Zn/O ratio	1.19	1.09	1.07	0.93	0.87
Al/Zn ratio	0	0.03	0.05	0.14	0.18
(Zn + Al)/O ratio	1.19	1.13	1.13	1.06	1.03
1/m	-	0.03	0.05	0.11	0.14

Considering the accuracy of the method (about 2%), we looked for Zn/O, Al/Zn and (Zn + Al)/O ratios of the films (Table 2).

Analyzing the results given in Table 2, we see that within the method accuracy, the films showed a good stoichiometry ((Zn + Al)/O ratio close to 1) but better for films with a larger Al fraction (m smaller). The Al/Zn ratio for m equal to 29 and 19 followed the ratio of ALD sequences.However, if the Al fraction was increased (samples AZO-3 and AZO-4), we observed deviation between Al/Zn and $1/m$. It looks like more reactive Al started to dominate and replace Zn. Formation of foreign phases may have occurred, limiting the "doping" method used in ALD.

Our previous investigations suggested that the increased fraction of Al affects also the growth mode of sample and sample crystallinity [25]. To verify/confirm this observation, we performed SEM (cross section images and top view) and XRD investigations. The relevant results are shown below. In Figure 2 we show the SEM images of ZnO and AZO layers deposited by the ALD at the conditions given in Table 2. A cross section on the left and top view on the right of the figure are presented, respectively. The results were compared with the ones obtained by us previously for the films grown at higher temperature [25]. Despite a lower growth temperature and considerably shorter purging times, they were quite similar. The ZnO layer grown at 160 °C showed columnar growth with a dominant c-axis orientation perpendicular to the surface of the films. Large grains (column diameters) were also observed.

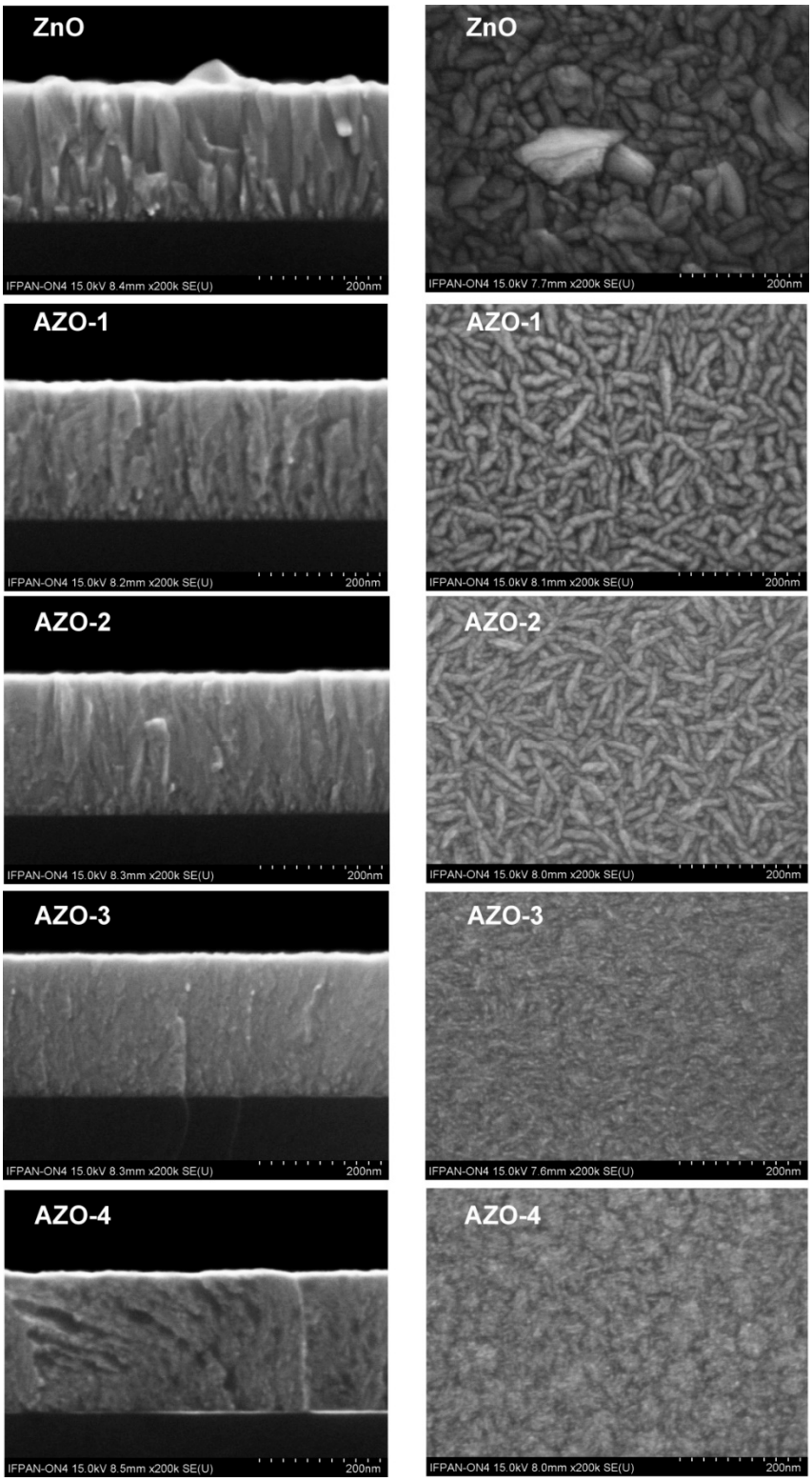

Figure 2. The SEM images of cross section (**left column**) and top view (**right column**) of ZnO and AZO layers on Si substrates.

A quite different surface morphology was observed for the AZO samples. For AZO samples, the growth was more chaotic with many of the columns in the plane of samples. Moreover, the grains size was diminishing as the Al concentration was increasing. For the AZO-4 sample, the majority of columns was in the plane of the sample, and an amorphous-like structure started to dominate, similarly as reported by us in reference [25].

To confirm this observation, we performed XRD investigations of AZO samples. The XRD patterns collected for AZO thin films prepared with different Al concentrations are shown in Figure 3. The crystalline state and crystal orientation of the films in fact changed with Al concentration, confirming the conclusions from SEM studies.

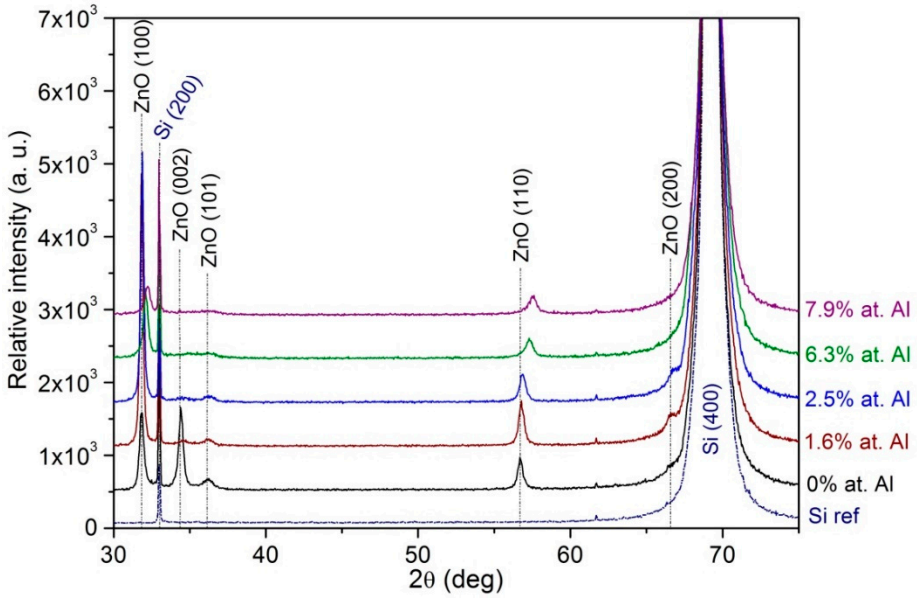

Figure 3. The XRD patterns collected for AZO films prepared with different Al concentration levels.

Undoped ZnO film exhibits a hexagonal structure. The sample was polycrystalline with randomly orientated grains showing (100), (002), (101) and (110) XRD peaks, with the (002) being the strongest [31]. As we investigated previously to obtain monocrystalline films, we needed a higher growth temperature [19] and longer purging times [23]. As Al_2O_3 interlayers were introduced (the method of doping with Al), the (002) XRD peak faded away, and the intensity of the (100) peak became dominant, with the maximum for a low Al fraction sample (1.6% Al). Evolution of ZnO peaks showed that introducing the Al_2O_3 interlayer affected the (002) growth, and the (100) XRD peak appeared to be the preferred growth direction. Similar results were reported by us [26] and in the references [32,33] for samples grown at slightly different conditions. It seems thus that the trend reported above is common for samples with Al.

The (100) and (110) ZnO peak parameters were analyzed, as these peaks were observed for all investigated Al concentrations. The 2θ position of both (100) and (110) peaks increased with increasing Al concentration in AZO films (Figure 4c). This indicates that the addition of Al to the ZnO layer reduced the inter-planar spacing in the (100) and (110) directions. It can be attributed to Al^{3+} ions vicariously replacing Zn^{2+} at random sites. In this context, the difference in the values of the ionic radius was important. The Zn^{2+} ionic radius was 72 pm, whereas that of the Al^{3+} was 54 pm. By the above, inter-planar distances can be reduced [30].

The total area of the (100) and (110) ZnO peaks (Figure 4a) had a maximal value at Al concentration equal to 1.6% and decreased as Al concentration increased to 7.9%. The grain size calculated for the (100) peak (we used the Scherrer approach [34,35] reached the maximum at 1.6–2.5 of at.% Al and then decreased, while for the (110) peak, it decreased as the at.% Al changed from 0 to 7.9% (see Figure 4b). Concluding, as the content of Al increased, the grains became smaller, and the diffraction peaks became weaker, i.e., the crystallization of AZO deteriorated, as also observed previously. In conclusion, when the Al content increased to 7.9%, AZO sampled tended to amorphize, the grains became smaller, and the diffraction peaks weakened. This is in line with the SEM results [25,26,33].

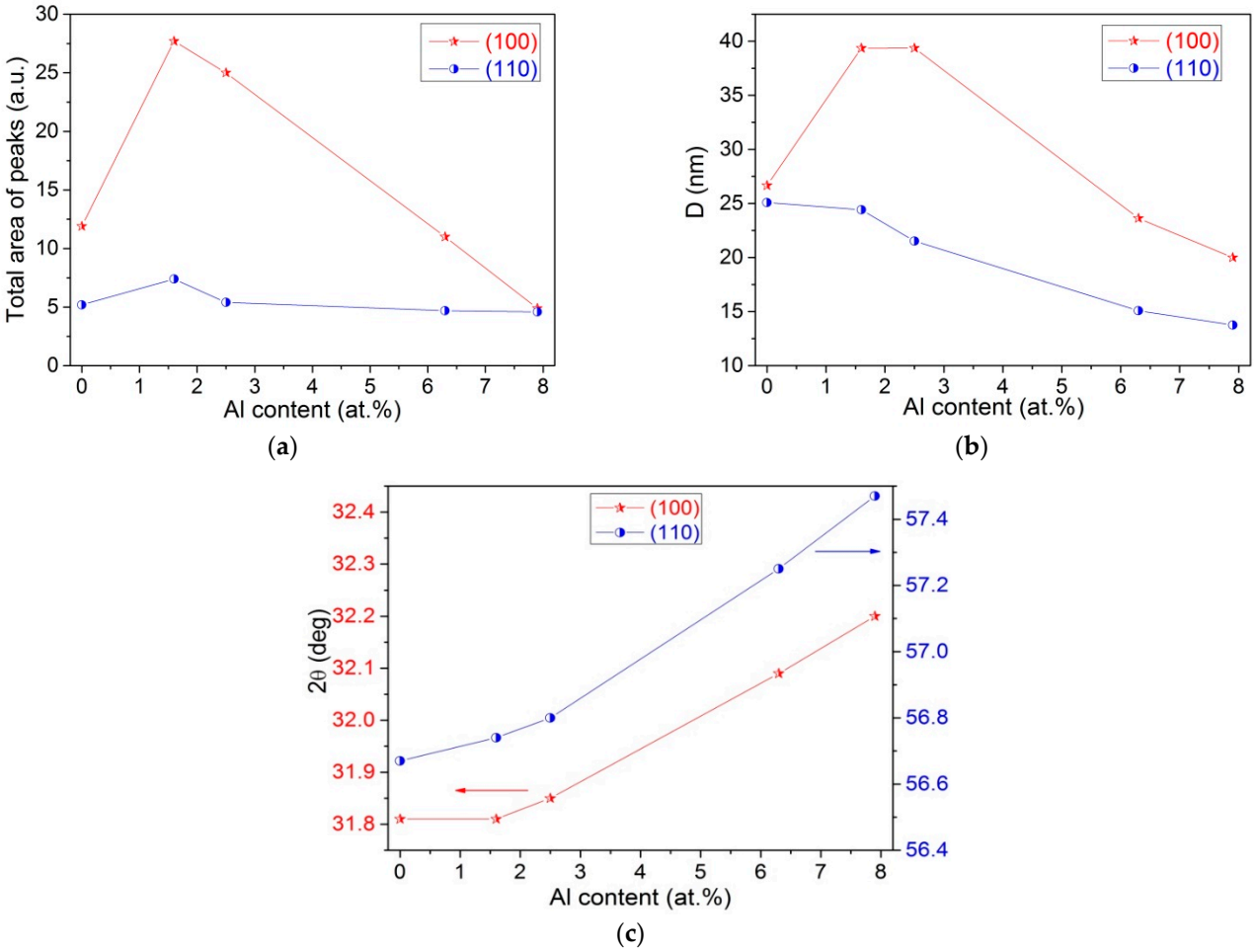

Figure 4. (**a**) The total peak area; (**b**) the grain size and (**c**) 2θ position of the (100) and (110) ZnO peaks, as a function of Al concentration (at.%).

Doping with Al is a way to improve sample conductivity to make them suitable for TCO applications. We thus looked for the efficiency of doping. The electrical parameters of ZnO and AZO layers determined from Hall measurements are shown in Table 3.

Table 3. Electrical parameters and band gap of ZnO and AZO layers with different Al concentrations, measured at room temperature (ρ—resistivity; μ—mobility of carriers; n—concentration of electrons; E_g—band gap).

	ZnO	AZO-1	AZO-2	AZO-3	AZO-4
ρ (Ωcm)	4.93×10^{-2}	7.59×10^{-3}	6.33×10^{-3}	2.04×10^{-2}	9.98×10^{-2}
μ (cm^2/Vs)	16.4	9.5	7.3	3.0	1.33
n (cm^{-3})	7.70×10^{18}	8.66×10^{19}	1.34×10^{20}	1.01×10^{20}	5.22×10^{19}
E_g (eV)	3.33	3.48	3.56	3.78	3.88

For the pure ZnO layer, the concentration of carriers at the level of 10^{18} cm^{-3}, mobility 16.4 cm^2/Vs and resistivity of 10^{-2} Ω cm were observed. These results were in line with the ones commonly reported by us for the ALD-grown ZnO films [20,22,24]. Aluminum doping of ZnO films improved their electrical properties, but only for low Al fractions. The relevant results are shown in Figure 5.

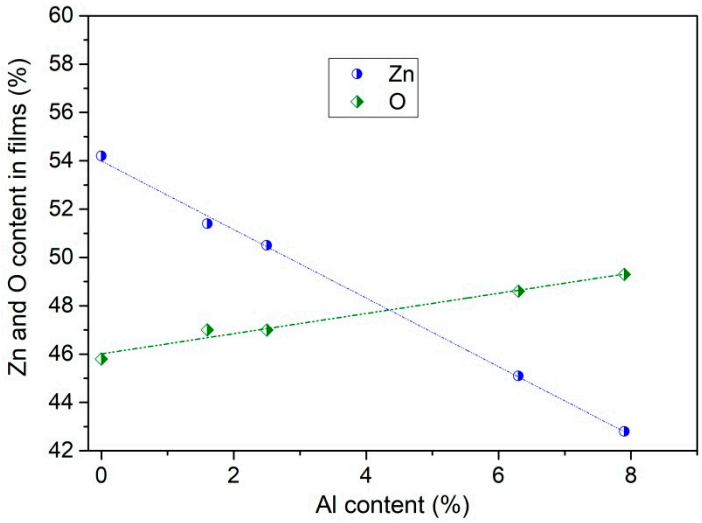

Figure 5. Relation between chemical composition of ZnO and AZO films on Al atomic content.

Figure 5 shows the variation of electrical resistivity ρ, carrier density n and Hall mobility μ as a function of the Al content in the films. With increasing Al content, the resistivity of the AZO films initially decreased up to 0.005 Ω.cm. This variation in resistivity was due to an increase in free carrier concentration as a result of electron released from the Al donors. Substitutional incorporation of Al^{3+} ions (after ionization of electrons) for Zn^{2+} cations was responsible for a marked enhancement of carrier concentration. However, interstitial doping could not be excluded. A broad minimum in resistivity was located between 1.5 and 6 at.% of Al. When the Al content exceeded 6 at.% of Al, ρ started to increase. This effect might be a result of clustering in a nonconducting form of Al_2O_3 related to the crystal disorder. The excess of Al entailed charge trapping rather than donor action. Such a possibility was suggested previously [32,36,37]. This is a possible explanation of the drop in free electron concentration. However, if created, the concentration of such traps must be low, since these clusters are not observed in the XRD investigations.

Another explanation was proposed in reference [25]. The decrease in the carrier concentration could have been due to compensation effects, i.e., because of native defects formation. From Figure 5, we can see that zinc content gradually decreased with increases in the Al content in the films. For the highest concentrations of Al dopant, this decline is significant. According to Kröger–Vink notation, when a small amount of Al_2O_3 is dissolved in ZnO [38], the Al atoms substitute the Zn sites:

$$Al_2O_3 \overset{2ZnO}{\rightarrow} 2Al_{Zn}^{\cdot} + 2O_O^x + O_i''$$

and when the larger amount of Al-dopant atoms is introduced into the ZnO matrix, the defect reaction is

$$Al_2O_3 \overset{3ZnO}{\rightarrow} 2Al_{Zn}^{\cdot} + 3O_O^x + Zn_i'' + 2V_{Zn}''$$

The increase in Al-doping level induced zinc interstitial (Z_{ni}) and zinc vacancy (V_{Zn}). It is likely that a large number of zinc vacancies will be created because their formation energy is relatively low [39]. The second expression shows that oxygen vacancies arise in the range of a higher level of doping with Al atoms. In addition, according to Wang et al. [40], higher doping levels of Al dopants reduced the formation energy of (V_{Zn}). Formation of such centers and likely of Al-V_{Zn} complexes may explain the decreased n-type doping efficiency. Furthermore, their high concentration should also affect the absorption spectrum, as discussed below.

The excess aluminum doping reduced the carrier concentration in the films. A consequence of this was an increase in resistivity. In Figure 6 is illustrated the decrease in the Hall mobility of the AZO films versus increases in Al content. The observed decrease

in grain size of the AZO films as it was seen in the SEM images and from XRD data (Figures 2 and 4b) also influenced carrier mobility. The decrease in the grain size increased grain boundary scattering, thus decreasing carrier mobility. Increased concentration of scattering centers (Al donors) also contributed to the mobility decrease.

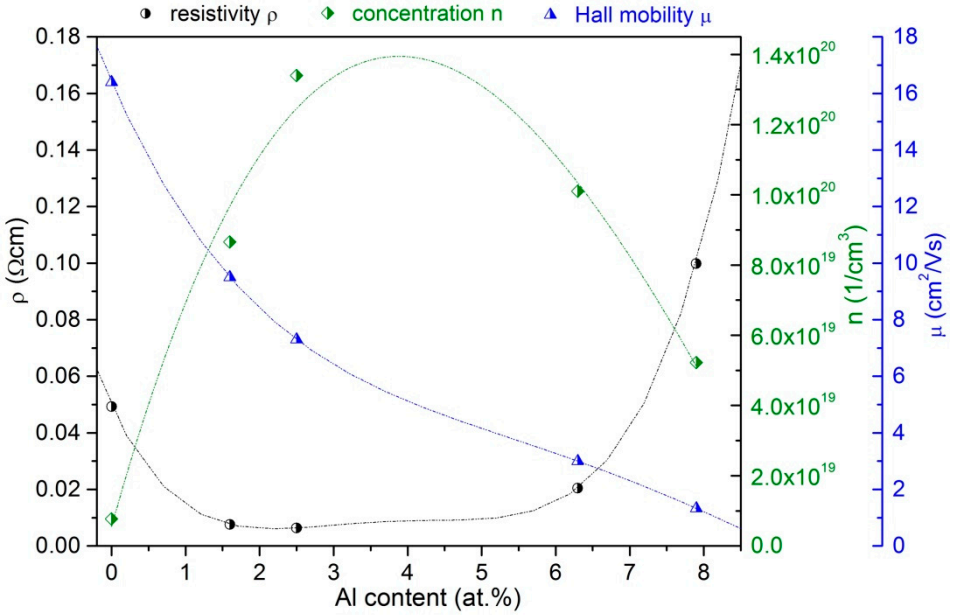

Figure 6. Dependence of electrical resistivity $\boldsymbol{\rho}$, carrier density $\boldsymbol{n}$ and Hall mobility $\boldsymbol{\mu}$ on Al content in the AZO films.

For small values of Al content in layers, the concentration $\boldsymbol{n}$ increased and the Hall mobility $\boldsymbol{\mu}$ decreased. After about 4% of Al content, both $\boldsymbol{n}$ and $\boldsymbol{\mu}$ decreased, but $\boldsymbol{n}$ definitely faster. We had to thus find an optimum between an increased free electron concentration and the drop of carrier mobility. The lowest resistivity was found for relatively low Al fractions in the samples—say between 2% and 6%. Moreover, this result differed from that reported previously [25]. In this reference a much sharper dependence of film resistivity on Al fraction was reported.

For TCO applications, the sample should be highly conductive but also transparent in a visible light range. We thus verified sample transparency after Al doping and determined the extinction parameters, which should be low for the films applied as transparent electrodes.

To determine the effect of Al doping on the optical properties of the films, we used two different measurement methods: ellipsometric spectroscopy (SE) (for the ZnO and AZO films deposited onto Si substrates), and transmission and reflection spectroscopy (T–R) in the case of films deposited onto glass substrates.

For the analysis and interpretation of ZnO and AZO thin films and optical properties, a multilayer model was used, in which the substrate was silicon (from the program library), and the investigated layer was fit using the general oscillator (GO) model. To obtain the dispersion relationships of optical constants n and k in oxides, the most popular model is the Cauchy model (the simplest model for nonabsorbing layers) [41]; oxide layers are also modeled using the Tanguy model [42], the Drude model [43] and the oscillator model [44,45]. Two Tauc–Lorentz oscillators were used [46]. The Tauc–Lorentz equation is as follows [47]:

$$\varepsilon_{T-L}(E) = \varepsilon_{n1} + i\varepsilon_{n2} \tag{1}$$

where

$$\varepsilon_{n2}(E) = \left[\frac{Amp_n E_{0n} B_{rn} (E - E_{gn})^2}{\left(E^2 - E_{0n}^2\right)^2 + B_{rn}^2 E^2} \cdot \frac{1}{E}\right] \text{ when } E > E_{gn} \tag{2}$$

$$\varepsilon_{n2}(E) = 0 \text{ when } E \leq E_{gn} \tag{3}$$

and

$$\varepsilon_{n1} = \frac{2}{\pi} P \int_{E_{gn}}^{\infty} \frac{\xi \varepsilon_{n2}(\xi)}{\xi^2 - E^2} d\xi \tag{4}$$

where ε_1 is the real part of dielectric function, and ε_2 is the imaginary part of dielectric function; the four fitting parameters are E_g, Amp_n, E_0 and B_r, and all are in units of energy (eV); P stands for the Cauchy principal part of the integral (Compleate EASETM Data Manual J.A. Woolam Co., Inc.). A parameterization of the optical functions of the material is connected with the imaginary part of the dielectric function and the Tauc density of states.

The dispersion relation of the refractive index $n(\lambda)$ with dielectric function and thickness of the layers were determined from the analysis of the data. The thickness determined from ellipsometric measurements was between 214 and 233 nm, i.e., very close to the intended thicknesses of the films based on the number of ALD "supercycles". The latter means that the growth rate was relatively weakly affected by the change of the ***m*** value and the fact that we used the same growth conditions for ZnO and Al_2O_3 deposition. Slightly thicker films were obtained when the ***m*** value was reduced, i.e., the number of Al_2O_3 cycles was increased.

The determined spectral dispersion of refractive index ***n*** (on the basis of SE measurements) for five samples is presented in Figure 7.

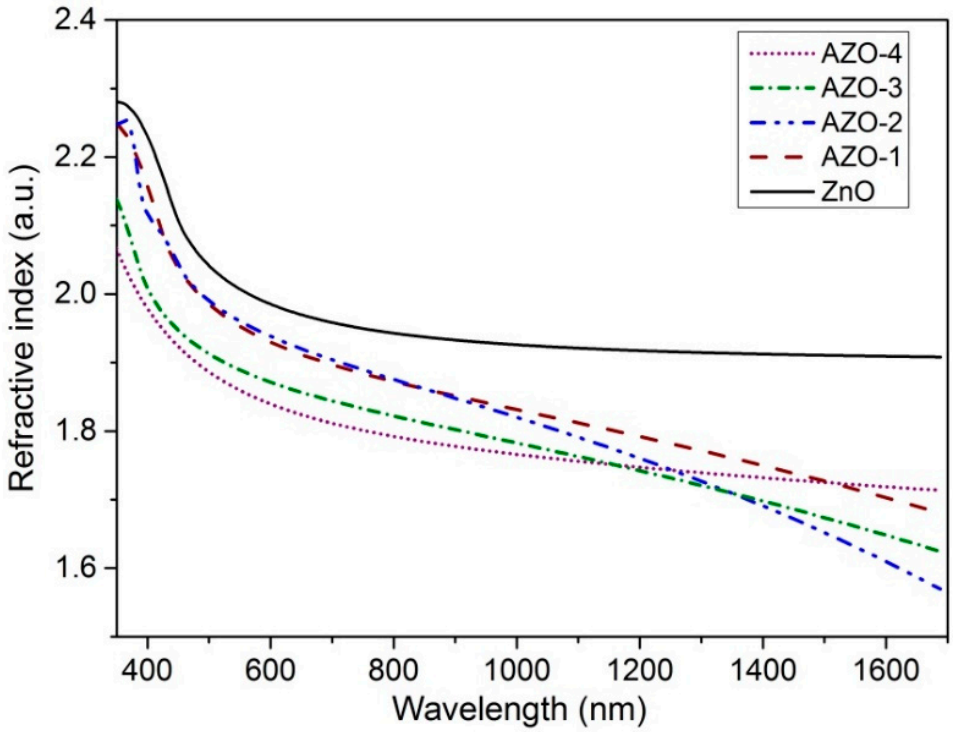

Figure 7. Spectral dependence of refractive index for samples with different contents of aluminum, from ellipsometric measurements (SE) using the general oscillator (GO) model.

The transmission spectra of ZnO and AZO1–4 films were also measured by use of a Perkin-Elmer spectrophotometer (T–R measurements). The obtained results are presented in Figure 8. All films were transparent with the average transmission in the visible light region (~85%). The absorption edge shifted towards higher energies with the increase of Al content, as we already reported previously [25].

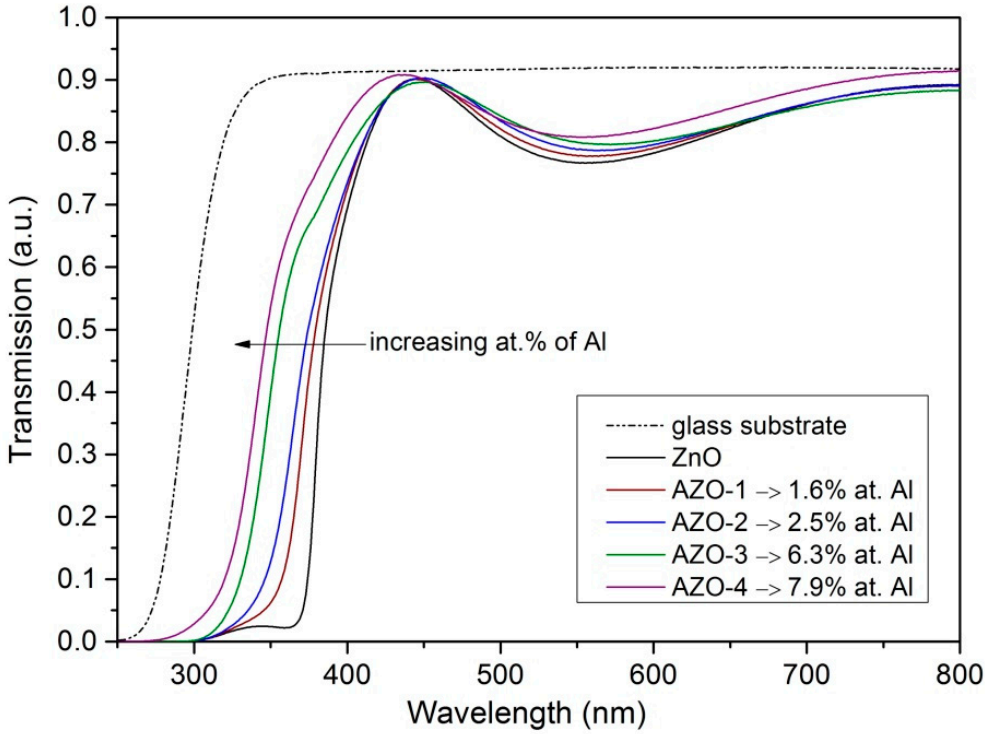

Figure 8. Transmission spectra of pure and Al-doped ZnO films on glass substrate at different Al contents.

A fit was performed to the experimental data. The Cauchy model was used. It describes the dispersion relation of refractive index $\boldsymbol{n}$ and extinction coefficient $\boldsymbol{k}$ of dielectric materials and semiconductors with relations described by Equations (5) and (6) [48]:

$$n(\lambda) = A + \frac{B}{\lambda^2} + \frac{C}{\lambda^4} \tag{5}$$

$$k(\lambda) = D \cdot \exp\left\{E\left[12400\left(\frac{1}{\lambda} - \frac{1}{F}\right)\right]\right\} \tag{6}$$

The model is adjusted using the A, B and C parameters. As D is marked the extinction coefficient amplitude, the exponent factor is labeled E and the band edge is tagged F. Due to the consideration of band gap absorption at the edge of the band gap, this empirical model is useful for ZnO thin films [49]. Film Wizard (Scientific Computing International, Carlsbad, CA, USA) software was used to analyze the transmission and reflection spectra. The three-phase model was applied to describe the material configuration, i.e., air/ZnO film/glass substrate where the glass substrate was 0.5 mm thick. The typical fitting results of the transmission and reflection spectra are shown in Figure 9.

Figure 10a,b show the variations of refractive index $\boldsymbol{n}$ and extinction coefficient $\boldsymbol{k}$ of the films with different aluminum contents for the spectral range 300–800 nm. For ZnO and Al-doped ZnO films, there was a noticeable increase in refractive index with increasing wavelength, but then (for longer wavelengths) it slowly decreased. These changes resulted from the increase and decrease in optical absorption. The reduction to zero extinction coefficient above 450 nm was significant, which makes the material suitable for TCO applications.

The $\boldsymbol{n}$ index in the weak absorption region (for λ larger than 400 nm) decreased progressively with the increase of Al fraction. This can be related to the known fact that Al impurity in ZnO acts as an effective n-type donor; thus, doping leads to the generation of free carriers. As the Al content increased, the carrier concentration in the AZO layers increased. The enhancement of carrier concentration resulted in the decrease of refractive

index [50]. For selected applications, the ability to control and change ***n*** of AZO films by changing the aluminum content is important.

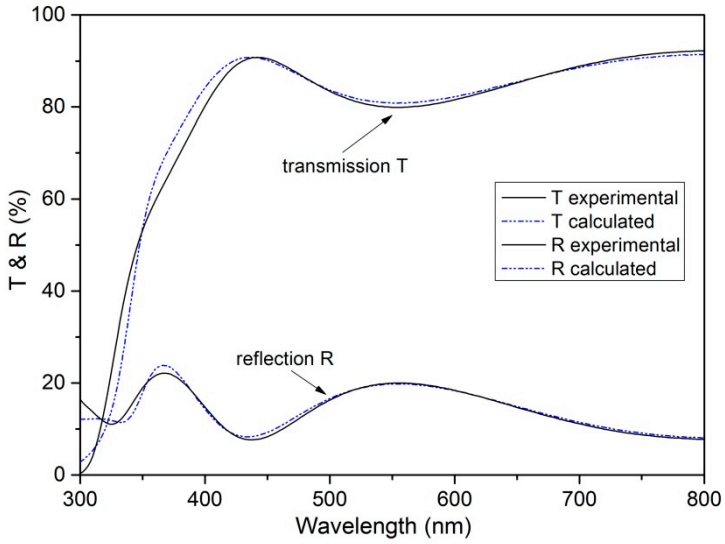

Figure 9. Transmission and reflection spectra vs. wavelength for sample AZO-4 (Al content 7.9%); experimental and calculated data (on the basis of Cauchy model).

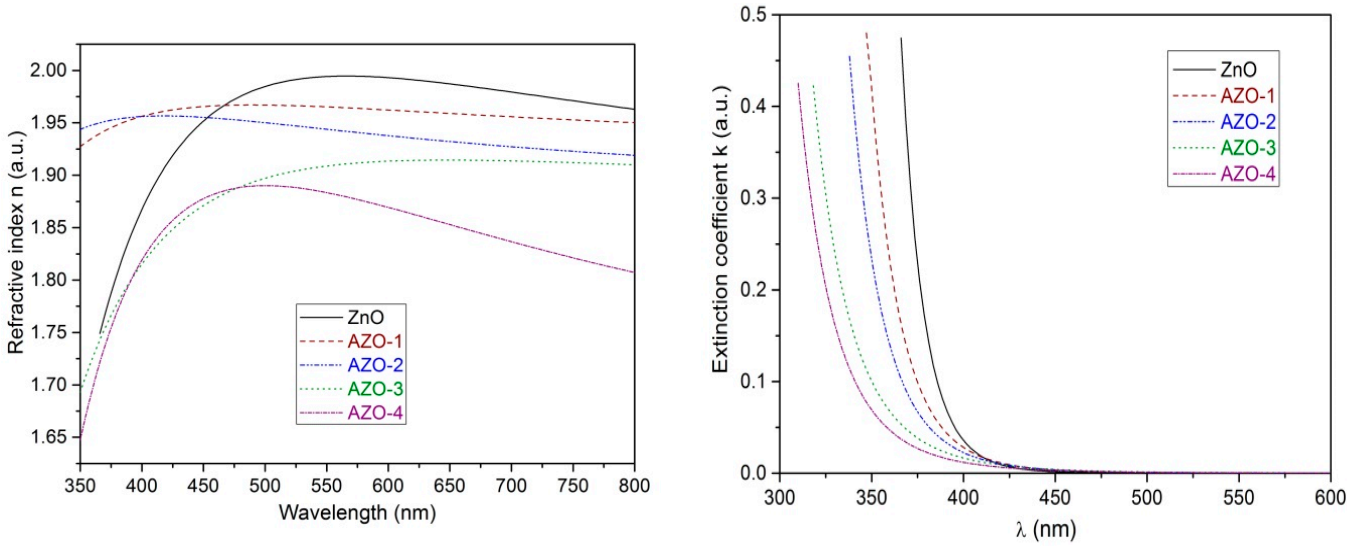

(**a**) (**b**)

Figure 10. The spectral dependences of: (**a**) the refractive index ***n*** and (**b**) the extinction coefficient ***k***, obtained by the use of the Cauchy model.

Table 4 contains the values of thickness and refractive index of ZnO and AZO films, calculated on the basis of both kinds of optical measurements: SE and T–R.

The optical energy gaps were estimated by using the equation for a direct allowed type band-to-band transition:

$$(\alpha h\nu)^2 = A(E - E_g) \quad (7)$$

where A is a constant, E_g is the optical energy gap and $\alpha = 4\pi k/\lambda$ is the optical absorption coefficient; α can be calculated from the extinction coefficient k.

Figure 11 shows a plot of $(\alpha h\nu)^2$ vs. the photon energy. The linear fitting allowed us to determine the sharp absorption edge of the AZO layers. The point where $(\alpha h\nu)^2$ equals zero indicates the E_g. This procedure may lead to some errors, since for larger Al

fractions, we observed a relative long tail at lower energies, and the linear part of the plot was relatively short.

Table 4. Main parameters from optical measurements (T–R and SE).

	Al Content (at.%)	Thickness from T–R (nm)	Thickness from SE (nm)	n from T–R for 600 nm	n from SE for 600 nm (on Base GO Model)
ZnO	0	214	214	2.01	1.98
AZO-1	1.6	211	218	1.92	1.93
AZO-2	2.5	213	220	1.94	1.92
AZO-3	6.3	225	231	1.93	1.86
AZO-4	7.9	228	233	1.85	1.81

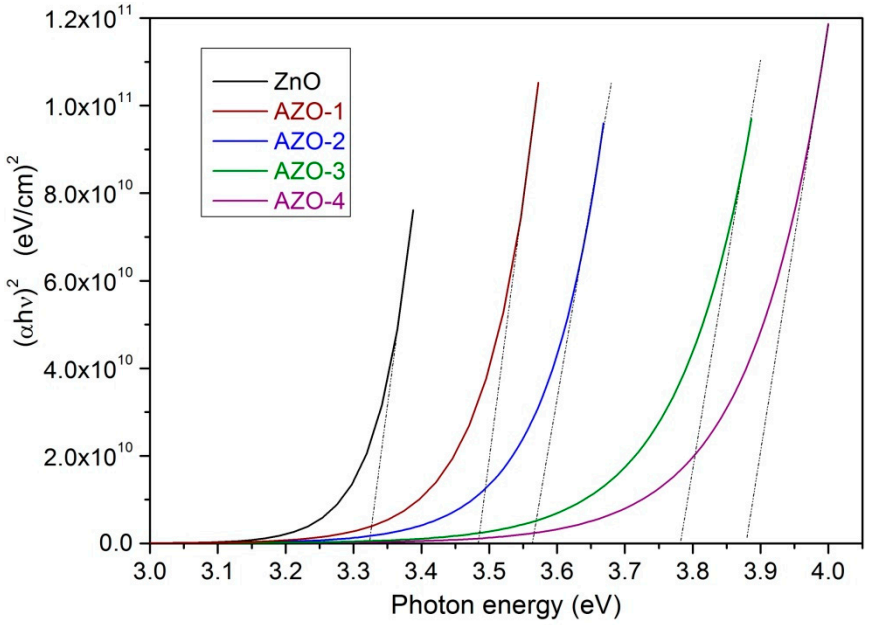

Figure 11. Energy gap for analyzed thin films, detected from Formula (7).

Despite some limitations of the method of E_g estimation, it was seen (see Figure 11) that the absorption edge shifted to the shorter wavelength region (larger energies) with increasing Al content. Similar results reported previously [25] were explained (for lower Al fractions) by the Burstein–Moss effect [51]. This is in line with the observed metallic-like conductivity of heavily doped AZO films. The widening of the optical band is related to the fact that optical transitions can only take place between the valence band and states in the conduction band above the Fermi level, which itself is related to the fact that states below the Fermi level are occupied by electrons.

Until now we used the language of doping, but once Al fraction is up to nearly 8% it is more like alloying than doping. Surprisingly, the results shown in Figure 12 were in line with this possibility. The optical band gap increased linearly with the Al fraction in the sample. The explanation of the observed large shift of the optical band gap by Burstein–Moss effect only is thus confusing.

To clear up this confusing situation, we repeated the approach used previously by us in reference [24]. The Burstein–Moss effect predicts the following relationship between an optical energy gap and a carrier concentration:

$$\Delta E_{BM} = \left(\frac{h^2}{8m^*}\right)\left(\frac{3n}{\pi}\right)^{\frac{2}{3}} \quad (8)$$

where h is Planck's constant, m^* is the effective mass of the electron and n is the carrier concentration.

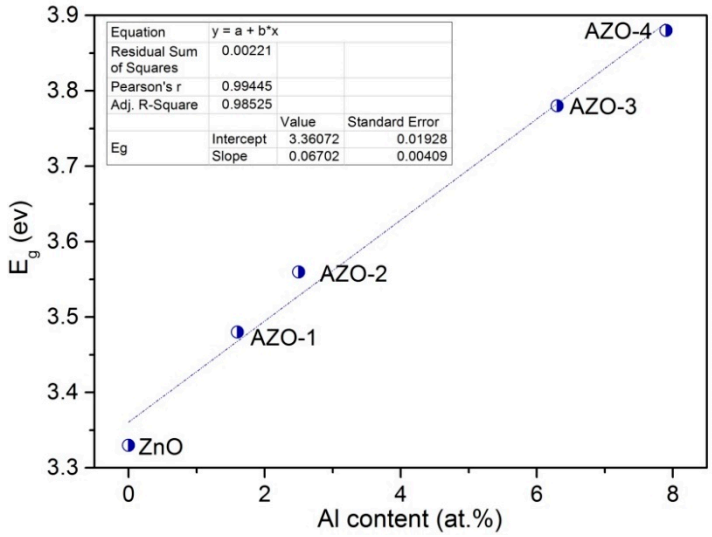

Figure 12. Optical band gap as a function of Al content in the analyzed films.

As can be seen from Figure 13, this dependence was valid up to 2.5 at.% of Al only. In addition to the Burstein–Moss band filling, band gap renormalization effects should also be taken into account. Band gap renormalization results from many body interactions and causes bandgap narrowing. The Jain model [52], which can be taken to estimate bandgap renormalization, is binding for AZO films also [53]. Based on Jain's analyses [52], the gap narrowing may be expressed in the form of $E_{BGN} = An^{1/3} + Bn^{1/4} + Cn^{1/2}$. The $n^{1/3}$, $n^{1/4}$ and $n^{1/2}$ dependencies correspond to the exchange energy of free electrons, their correlation energy and the electron–ion interaction energy, respectively. A and B coefficients are theoretically calculated, and C is a fitting parameter. However, in our case only three points were available for the calculations (up to 2.5 at.% Al), which made it difficult to compare the contributions of Burstein–Moss and band gap narrowing effects to the variation of band gap values with respect to electron concentration. That is why we gave up on the calculations with little data availability.

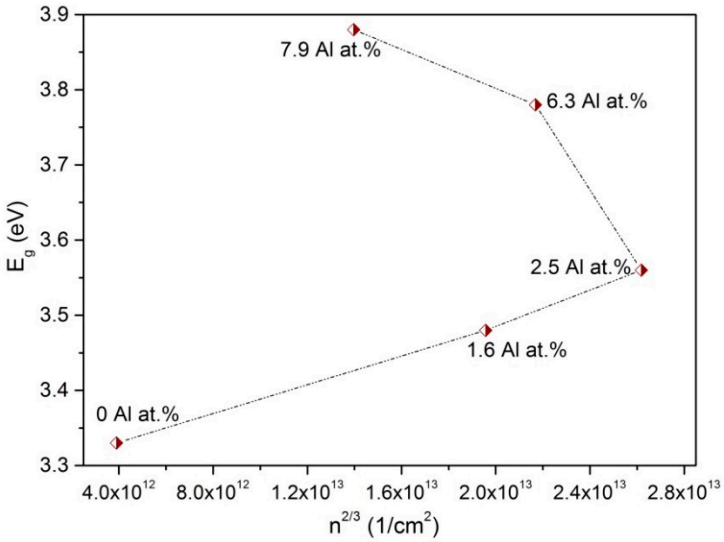

Figure 13. Optical band gap vs. (carrier concentration n)$^{2/3}$ for AZO films.

Above 2.5 at.% of Al doping, the E_g does not depend linearly on $n^{2/3}$. There is a decrease in n as E_g increases further. This indicates a change in the creation of free carriers in the AZO layers. A model assuming alloy formation is not also supported by the that the Al/Zn ratio followed the ratio of ALD sequences only for m parameter equal to 29 and 19 (see Table 2). However, if the Al fraction increases (samples AZO-3 and AZO-4), we observe a deviation between Al/Zn and $1/m$. One possibility is that formation of foreign phases may occur, limiting the "doping" method used in the ALD. If such foreign phases (e.g., Al_2O_3) are formed, their concentration must be low, below the detection limit of the XRD. Summarizing, the observed large shift of the optical band gap still remains puzzling, with the Burstein–Moss effect possible but only for samples with low Al fractions.

4. Conclusions

ALD technology enables precise control of Al content in AZO layers for films grown with Al fractions of up to 3%. Unfortunately, the layer morphology and electrical parameters strongly depend on Al content in the AZO films grown by the ALD. The samples with Al fractions above ~3% tend to be more disordered, the columnar ZnO structure is no longer observed and the resistivity of samples increases instead of decreasing. The large increase of the optical band gap is observed, but the explanation of this effect is not straightforward. Only for the AZO films with low Al fractions can the Burstein–Moss effect be observed. Differences in the activity of Al and Zn may account for the observed problems with uniform doping/alloying films with larger Al fractions. Nevertheless AZO films with Al fractions up to 2–3% show the required optical and electrical properties for their use in photovoltaics as transparent electrodes. It is also likely that samples with larger Al fractions may be useful (e.g., for transparent electrodes in UV LEDs), but their preparation must be optimized. Post-growth annealing may be useful, since it improves Al distribution in the films [26].

Author Contributions: Conceptualization: M.G., T.S. and R.P.; Formal analysis: B.S., T.S., R.P. and M.G.; Investigation: B.S., W.P., H.C., G.L., R.P. and B.S.W.; Methodology: H.C., T.S., B.S.W. and M.G.; Project administration: M.G.; Validation: B.S.; Visualization: B.S.; Writing – original draft: R.P., M.G., T.S. and B.S.; Writing – review & editing: B.S. All authors have read and agreed to the published version of the manuscript.

Funding: This work was partially supported by the Polish Ministry of Science and Higher Education under subvention funds of the Department Institutional Review Board Statement of Electronics of AGH University of Science and Technology (AGH grant number 16.16.230.434) and by the National Centre for Research and Development project TECHMATSTRATEG1/347012/NCBR/2017 and TECHMATSTRATEG1/347431/14/NCBR/2018.

Institutional Review Board Statement: Not applicable.

Informed Consent Statement: Not applicable.

Conflicts of Interest: The authors declare no conflict of interest.

References

1. Jagadish, C.; Pearton, S.J. (Eds.) *Zinc Oxide Bulk, Thin Films and Nanostructures*; Elsevier: Oxford, UK, 2006.
2. Duenow, J.N.; Gessert, T.A.; Wood, D.M.; Barnes, T.M.; Young, M.; To, B.; Coutts, T.J. Transparent conducting zinc oxide thin films doped with aluminum and molybdenum. *J. Vac. Sci. Technol. A* **2007**, *25*, 955–960. [CrossRef]
3. Minami, T.; Nanto, H.; Takata, S. Highly conductive and transparent aluminum doped zinc oxide thin films prepared by RF magnetron sputtering. *Jpn. J. Appl. Phys.* **1984**, *23*, L280–L282. [CrossRef]
4. Minami, T. Transparent conducting oxide semiconductors fortransparent electrodes. *Semicond. Sci. Technol.* **2005**, *20*, S35. [CrossRef]
5. Kim, H.; Gilmore, C.M.; Pique, A.; Horwitz, J.S.; Mattoussi, H.; Murata, H.; Kafafi, Z.H.; Chrisey, D.B. Electrical, optical, and structural properties of indium–tin–oxide thin films for organic light-emitting devices. *J. Appl. Phys.* **1999**, *86*, 6451–6461. [CrossRef]
6. Coutts, T.J.; Young, D.L.; Li, X.; Mulligan, W.P.; Wu, X.J. Search for improved transparent conducting oxides: A fundamental investigation of CdO, Cd_2SnO_4, and Zn_2SnO_4. *Vac. Sci. Technol. A* **2000**, *18*, 2646. [CrossRef]

7. Minami, T.; Suzuki, S.; Miyata, T. Transparent conducting impurity-co-doped ZnO:Al thin films prepared by magnetron sputtering. *Thin Solid Films* **2001**, *53*, 398–399. [CrossRef]
8. Suzuki, A.; Matsushita, T.; Wada, N.; Sakamoto, Y.; Okuda, M. Transparent conducting Al-doped ZnO thin films prepared by pulsed laser deposition. *Jpn. J. Appl. Phys.* **1996**, *35*, L56. [CrossRef]
9. Martin, A.; Espinos, J.P.; Justo, A.; Holgado, J.P.; Yubero, F.; Gonzalez-Elipe, A.R. Preparation of transparent and conductive Al-doped ZnO thin films by ECR plasma enhanced CVD. *Surf. Coat. Technol.* **2002**, *289*, 151–152. [CrossRef]
10. Ohyama, M.; Kozuka, H.; Yoko, T.J. Sol-gel preparation of transparent and conductive aluminum-doped zinc oxide films with highly preferential crystal orientation. *Am. Ceram. Soc.* **1998**, *81*, 1622–1632. [CrossRef]
11. Amakali, T.; Daniel, L.S.; Uahengo, V.; Dzade, N.Y.; de Leeuw, N.H. Structural and optical properties of ZnO thin films prepared by molecular precursor and sol–gel methods. *Crystals* **2020**, *10*, 132. [CrossRef]
12. Bosio, A.; Romeo, N.; Mazzamuto, S.; Canevari, V. Polycrystalline CdTe thin films for photovoltaic applications. *Prog. Cryst. Growth Charact.* **2006**, *52*, 247–279. [CrossRef]
13. Elmer, K. Resistivity of polycrystalline zinc oxide films: Current status and physical limit. *J. Phys D Appl. Phys.* **2001**, *34*, 3097–3108. [CrossRef]
14. Pietruszka, R.; Witkowski, B.S.; Zielony, E.; Gwozdz, K.; Placzek-Popko, E.; Godlewski, M. ZnO/Si heterojunction solar cell fabricated by atomic layer deposition and hydrothermal methods. *Sol. Energy* **2017**, *155*, 1282–1288. [CrossRef]
15. Kessler, J.; Bodegard, M.; Hedstrom, J.; Stolt, L. Baseline Cu(In, Ga)Se_2 device production: Control and statistical significance. *Sol. Energy Mater. Sol. Cells* **2001**, *67*, 67–76. [CrossRef]
16. Suntola, T. Atomic layer epitaxy. *Mater. Sci. Rep.* **1989**, *4*, 261–312. [CrossRef]
17. Ritala, M.; Leskelä, M.; Dekker, J.-D.; Mutsaers, C.; Soininen, P.J.; Skarp, J. Perfectly conformal TiN and Al_2O_3 films deposited by atomic layer deposition. *Chem. Vap. Depos.* **1999**, *5*, 7–9. [CrossRef]
18. Kukli, K.; Ritala, M.; Leskelä, M. Development of dielectric properties of niobium oxide, tantalum oxide, and aluminum oxide based nanolayered materials. *J. Electrochem. Soc.* **2001**, *148*, F35–F41. [CrossRef]
19. Kopalko, K.; Godlewski, M.; Domagała, J.Z.; Łusakowska, E.; Minikayev, R.; Paszkowicz, W.; Szczerbakow, A. Monocrystalline ZnO films on GaN/Al_2O_3 by atomic layer epitaxy in gas flow. *Chem. Mater.* **2004**, *16*, 1447–1450. [CrossRef]
20. Godlewski, M.; Guziewicz, E.; Szade, J.; Wójcik-Głodowska, A.; Krajewski, T.; Kopalko, K.; Jakieła, R.; Yatsunenko, S.; Przeździecka, E.; Kruszewski, P.; et al. Vertically stacked non-volatile memory devices–material considerations. *Microelectron. Eng.* **2008**, *85*, 2434–2438. [CrossRef]
21. Puurunen, R.L. A short history of atomic layer deposition: Tuomo Suntola's atomic layer epitaxy. *Chem. Vap. Depos.* **2014**, *20*, 332–344. [CrossRef]
22. Godlewski, M.; Guziewicz, E.; Łuka, G.; Krajewski, T.; Łukasiewicz, M.; Wachnicki, Ł.; Wachnicka, A.; Kopalko, K.; Sarem, A.; Dalati, B. ZnO layers grown by atomic layer deposition: A new material for transparent conductive oxide. *Thin Solid Films* **2009**, *518*, 1145–1148. [CrossRef]
23. Kowalik, I.A.; Guziewicz, E.; Kopalko, K.; Yatsunenko, S.; Wójcik-Głodowska, A.; Godlewski, M.; Dłużewski, P.; Łusakowska, E.; Paszkowicz, W. Structural and optical properties of low-temperature ZnO films grown by atomic layer deposition with diethylzinc and water precursors. *J. Cryst. Growth* **2009**, *311*, 1096–1101. [CrossRef]
24. Guziewicz, E.; Godlewski, M.; Krajewski, T.; Wachnicki, Ł.; Szczepanik, A.; Kopalko, K.; Wójcik-Głodowska, A.; Przeździecka, E.; Paszkowicz, W.; Łusakowska, E.; et al. ZnO grown by atomic layer deposition: A material for transparent electronics and organic heterojunctions. *J. Appl. Phys.* **2009**, *105*, 122413. [CrossRef]
25. Luka, G.; Krajewski, T.A.; Witkowski, B.S.; Wisz, G.; Virt, L.S.; Guziewicz, E.; Godlewski, M. Aluminum-doped zinc oxide films grown by atomic layer deposition for transparent electrode applications. *J. Mater. Sci. Mater. Electron.* **2011**, *22*, 1810–1815. [CrossRef]
26. Luka, G.; Wachnicki, Ł.; Witkowski, B.S.; Krajewski, T.A.; Jakiela, R.; Guziewicz, E.; Godlewski, M. The uniformity of Al distribution in aluminum-doped zinc oxide films grown by atomic layer deposition. *Mat. Sci. Eng. B-Adv.* **2011**, *176*, 237–241. [CrossRef]
27. Fujiwara, H. *Spectroscopic Ellipsometry: Principles and Applications*; John Wiley & Sons: Chichester, UK; Maruzen Co., Ltd.: Tokyo, Japan, 2007.
28. Azzam, R.M.A.; Bashara, N.M. *Ellipsometry and Polarized Light*; North Holland Publishing Company: Amsterdam, The Netherlands, 1977; pp. 37–54.
29. Woollam, J.A.; Johs, B.; Herzinger, C.M.; Hilfiker, J.; Synowicki, R.; Bungay, C.L. Overview of variable angle spectroscopic ellipsometry (VASE), part I: Basic theory and typical applications. *Crit. Rev.* **1999**, *CR72*, 3–28. [CrossRef]
30. J.A. Woollam Co., Inc. *Complete Easy Data Analysis Manual*; J.A. Woollam Co., Inc.: Lincoln, UK, 2008; pp. 18–22.
31. Quemener, V.; Alnes, M.; Vines, L.; Rauwel, P.; Nilsen, O.; Fjellvag, H.; Monakhov, E.V.; Svensson, B.G. The work function of n-ZnO deduced from heterojunctions with Si prepared by ALD. *J. Phys. D Appl. Phys.* **2012**, *45*, 315101. [CrossRef]
32. Banerjee, P.; Lee, W.-J.; Bae, K.-R.; Lee, S.B.; Rubloff, G.W. Structural, electrical, and optical properties of atomic layer deposition Al-doped ZnO films. *J. Appl. Phys.* **2010**, *108*, 043504. [CrossRef]
33. Zhai, C.-H.; Zhang, R.-J.; Chen, X.; Zheng, Y.-X.; Wang, S.-Y.; Liu, J.; Dai, N.; Chen, L.-Y. Effects of Al doping on the properties of ZnO thin films deposited by atomic layer deposition. *Nanoscale Res. Lett.* **2016**, *11*, 1–8. [CrossRef] [PubMed]

34. Scherrer, P. Bestimmung der inneren Struktur und der Größe von Kolloidteilchen mittels Röntgenstrahlen. *Goettinger Nachr.* **1918**, *26*, 98.
35. Hsu, J.-C.; Chen, Y.-Y. Comparison of the optical and electrical properties of Al-Doped ZnO films using a lorentz model. *Coatings* **2019**, *9*, 4. [CrossRef]
36. Hu, J.; Gordon, R.G. Textured aluminum-doped zinc oxide thin films from atmospheric pressure chemical-vapor deposition. *J. Appl. Phys.* **1992**, *71*, 880–889. [CrossRef]
37. Aktaruzzaman, A.F.; Sharma, G.L.; Malhotra, L.K. Electrical, optical and annealing characteristics of ZnO:Al films prepared by spray pyrolysis. *Thin Solid Films* **1991**, *198*, 67–74. [CrossRef]
38. Carter, C.B.; Norton, M.G. *Ceramic Materials: Science and Engineering*; Springer Science + Buisness Media: New York, NY, USA, 2013. [CrossRef]
39. Willander, M.; Nur, O.; Sadaf, J.R.; Qadir, M.I.; Zaman, S.; Zainelabdin, A.; Bano, N.; Hussain, I. Luminescence from zinc oxide nanostructures and polymers and their hybrid devices. *Materials* **2010**, *3*, 2643–2667. [CrossRef]
40. Wang, Q.J.; Wang, J.B.; Zhong, X.L.; Tan, Q.H.; Hu, Z.; Zhou, Y.C. Magnetism mechanism in ZnO and ZnO doped with nonmagnetic elements X (X = Li, Mg, and Al): A first-principles study. *Appl. Phys. Lett.* **2012**, *100*, 132407. [CrossRef]
41. Li, Q.H.; Zhu, D.; Liu, W.; Liu, Y.; Ma, X.C. Optical properties of Al-doped ZnO thin films by ellipsometry. *Appl. Surf. Sci.* **2008**, *254*, 2922–2926. [CrossRef]
42. Bouzourâa, M.-B.; Battie, Y.; Dalmasso, S.; Zaïbi, M.-A.; Oueslati, M.; En Naciri, A. Temperature dependent optical properties of ZnO thin film using ellipsometry and photoluminescence. *Superlattices Microst.* **2018**, *117*, 457–468. [CrossRef]
43. Fricke, L.; Boentgen, T.; Lorbeer, J.; Bundesmann, C. An extended Drude model for the in-situ spectroscopic ellipsometry analysis of ZnO thin layers and surface modifications. *Thin Solid Films* **2014**, *571*, 437–441. [CrossRef]
44. Pandey, S.K.; Awasthi, V.; Verma, S.; Gupta, M.; Mukherjee, S. Spetroscopic ellipsometry study on electrical and elemental properties of Sb-doped ZnO thin films. *Curr. Appl. Phys.* **2015**, *15*, 479–485. [CrossRef]
45. Aghgonbad, M.M.; Sedghi, H. Influence of annealing temperature on optical properties of zinc oxide thin films analyzed by spectroscopic ellipsometry method. *Chin. J. Phys.* **2018**, *56*, 2129–2138. [CrossRef]
46. Ferlauto, A.S.; Ferreira, G.M.; Pearce, J.M.; Wronski, C.R.; Collins, R.W. Analytical model for the optical functions of amorphous semiconductors from the near-infrared to ultraviolet: Applications in thin film photovoltaics. *J. Appl. Phys.* **2002**, *92*, 2424–2436. [CrossRef]
47. Jellison, G.E.; Modine, F.A. Parameterization of the optical functions of amorphous materials in the interband region. *Appl. Phys. Lett.* **1996**, *69*, 371–373. [CrossRef]
48. Tompkins, H.G.; Mc Gahan, W.A. *Spectroscopic Ellipsometry and Reflectometry: A User's Guide*; John Wiley & Sons, Inc.: New York, NY, USA, 1999; p. 93.
49. Liu, Y.C.; Hsieh, I.H.; Tung, S.K. Extraction of optical constants of zinc oxide thin films by ellipsometry with various models. *Thin Solid Films* **2006**, *510*, 32–38. [CrossRef]
50. Xue, S.W.; Zu, X.T.; Zheng, W.G.; Deng, H.X.; Xiang, X. Effects of Al doping concentration on optical parameters of ZnO:Al thin films by sol gel technique. *Phys. B Phys. Condens. Matter* **2006**, *381*, 209–213. [CrossRef]
51. Burstein, E. Anomalous optical absorption limit in InSb. *Phys. Rev.* **1954**, *93*, 632–633. [CrossRef]
52. Jain, S.C.; McGregor, J.M.; Roulston, D.J. Band-gap narrowing in novel III-V semiconductors. *J. Appl. Phys.* **1990**, *69*, 3747. [CrossRef]
53. Lu, J.G.; Fujita, S.; Kawaharamura, T.; Nishinaka, H.; Kamada, Y.; Ohshima, T.; Ye, Z.Z.; Zeng, Y.J.; Zhang, Y.Z.; Zhu, L.P.; et al. Carrier concentration dependence of band gap shift in n-type ZnO:Al films. *J. Appl. Phys.* **2007**, *101*, 083705. [CrossRef]